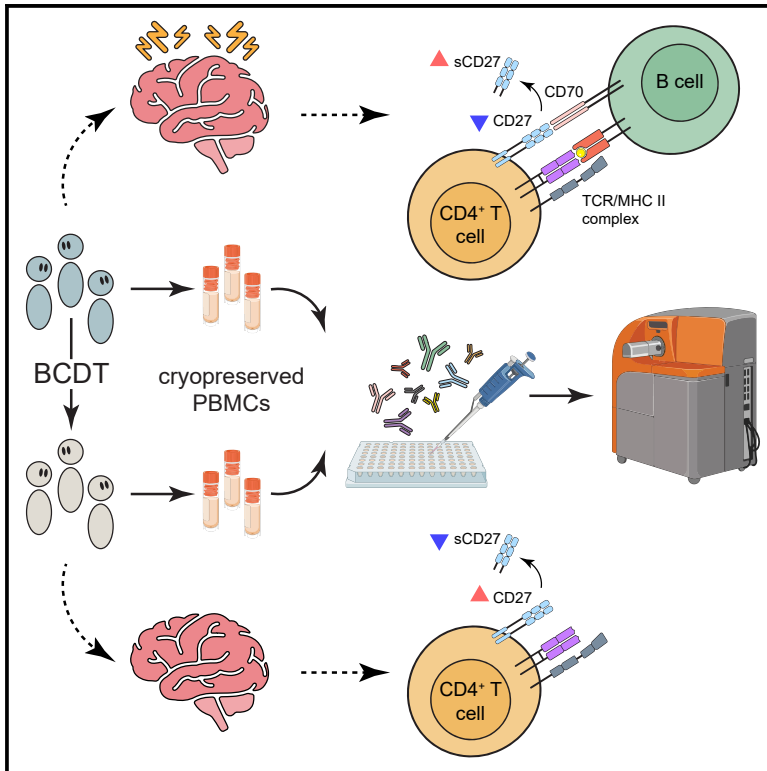**Report**

B cell depletion attenuates CD27 signaling of T helper cells in multiple sclerosis

Graphical abstract

Authors

Can Ulutekin, Edoardo Galli,
Bettina Schreiner, ..., Tobias Derfuss,
Florian Ingelfinger, Burkhard Becher

Correspondence

becher@immunology.uzh.ch

In brief

Ulutekin et al. analyze BCDT effects on MS immune landscape, revealing elevated surface CD27 levels in T helper cells post-treatment, suggesting reduced CD27/CD70 pathway activation. In MS, CD70-expressing B cells localize in MS lesion sites, suggesting that BCDT efficacy may partly hinge upon disruption of B-T helper cell interactions.

Highlights

- B cell-depleting therapies (BCDTs) lead to elevated surface CD27 in T helper (Th) cells

- BCDTs decrease the frequency of circulating T follicular helper-like (Tfh-like) cells

- CD27-expressing Th cells and CD70-expressing B cells co-localize in MS lesions

CelPress

Report

B cell depletion attenuates CD27 signaling of T helper cells in multiple sclerosis

Can Ulutekin,[1,9] Edoardo Galli,[1,2,9] Bettina Schreiner,[1,3] Mohsen Khademi,[4] Ilaria Callegari,[2] Fredrik Piehl,[4] Nicholas Sanderson,[2] Daniel Kirschenbaum,[5] Sarah Mundt,[1] Massimo Filippi,[6,7] Roberto Furlan,[8] Tomas Olsson,[4] Tobias Derfuss,[2] Florian Ingelfinger,[1,10] and Burkhard Becher[1,10,11,*]

[1]Institute of Experimental Immunology, University of Zurich, Winterthurerstrasse 190, 8057 Zurich, Switzerland
[2]Multiple Sclerosis Center, Neurologic Clinic and Policlinic, Department of Biomedicine and Research Center for Clinical Neuroimmunology and Neuroscience Basel, University Hospital Basel, University of Basel, Petersgraben 4, 4031 Basel, Switzerland
[3]Department of Neurology, University Hospital Zurich, Rämistrasse 100, 8091 Zurich, Switzerland
[4]Neuroimmunology Unit, Department of Clinical Neuroscience, Karolinska Institutet, Visionsgatan 18A, 171 76 Stockholm, Sweden
[5]Institute of Neuropathology, University Hospital Zurich, University of Zurich, Schmelzbergstrasse 12, 8091 Zurich, Switzerland
[6]Neurology Unit, Neurorehabilitation Unit, Neurophysiology Service, and Neuroimaging Research Unit, Division of Neuroscience, IRCCS San Raffaele Scientific Institute, Milan, Via Olgettina n. 60 – 20132, Italy
[7]Vita-Salute San Raffaele University, Milan, Via Olgettina n. 60 – 20132, Italy
[8]Clinical Neuroimmunology Unit, Institute of Experimental Neurology, Division of Neuroscience, IRCCS San Raffaele Scientific Institute, Via Olgettina n. 60 – 20132, Milan, Italy
[9]These authors contributed equally
[10]These authors contributed equally
[11]Lead contact
*Correspondence: becher@immunology.uzh.ch
https://doi.org/10.1016/j.xcrm.2023.101351

SUMMARY

Multiple sclerosis is a chronic inflammatory disease of the central nervous system. Whereas T cells are likely the main drivers of disease development, the striking efficacy of B cell-depleting therapies (BCDTs) underscore B cells' involvement in disease progression. How B cells contribute to multiple sclerosis (MS) pathogenesis—and consequently the precise mechanism of action of BCDTs—remains elusive. Here, we analyze the impact of BCDTs on the immune landscape in patients with MS using high-dimensional single-cell immunophenotyping. Algorithm-guided analysis reveals a decrease in circulating T follicular helper-like (Tfh-like) cells alongside increases in CD27 expression in memory T helper cells and Tfh-like cells. Elevated CD27 indicates disrupted CD27/CD70 signaling, as sustained CD27 activation in T cells leads to its cleavage. Immunohistological analysis shows CD70-expressing B cells at MS lesion sites. These results suggest that the efficacy of BCDTs may partly hinge upon the disruption of Th cell and B cell interactions.

INTRODUCTION

Multiple sclerosis (MS) is an immune-mediated disease characterized by demyelination of the central nervous system (CNS), where disease progression results from a complex interplay between partially understood neurodegenerative processes and inflammatory episodes. Traditionally, MS was considered a T cell-mediated disease based on evidence inferred from animal models of neuroinflammation.[1,2] However, therapies targeting exclusively T lymphocytes in patients demonstrated only weak clinical efficacy.[3] More recent evidence supports the involvement of B cells in the disease pathogenesis and progression of MS. One of the most convincing findings highlighting the critical role of B cells in the disease has been the high response rate of B cell-depleting therapies (BCDTs) in ameliorating MS.[4–6] These findings have shifted the perception of the disease toward mechanisms in which the interplay between B and T cells takes a more prominent role.[7]

Despite the impressive clinical efficacy of BCDTs in suppressing inflammatory disease activity in MS, their precise mechanism of action remains unclear and is an area of active research.[8] Removal of the total circulating immunoglobulin fraction via plasmapheresis[9,10] or interfering with potentially pathogenic antibodies via intravenous immune globulin (IVIG) injections[11–13] has shown limited efficacy. Furthermore, anti-CD20-mediated BCDTs do not target plasma cells and have minimal effects on antibody titers.[6] Thus, it appears likely that the success of BCDTs depends on B cell activities other than antibody production, such as cytokine secretion, antigen presentation, or co-stimulation. Several studies report upregulation of pro-inflammatory cytokines and a concomitant downregulation of immunoregulatory cytokines in B cells of MS.[14–20] Apart from cytokine production, B cells are antigen-presenting cells (APCs) and can efficiently prime T cells.[21] Accordingly, polymorphisms in major histocompatibility complex (MHC) genes demonstrate the strongest
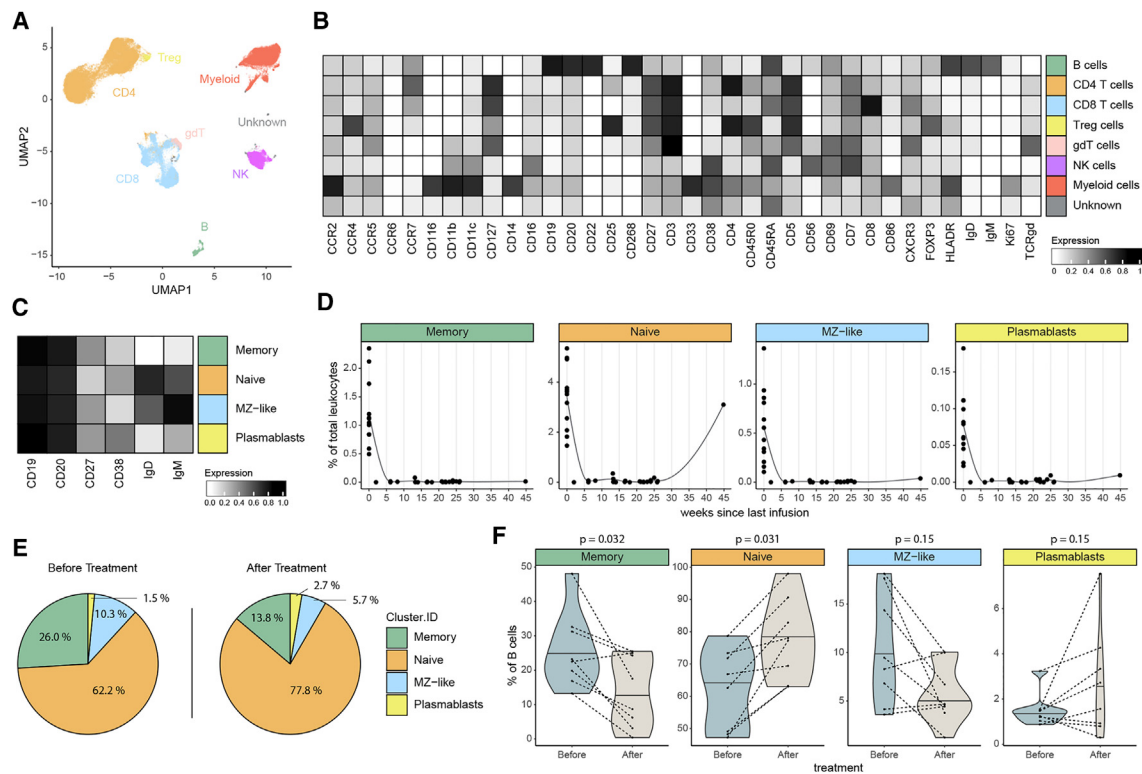
Figure 1. BCDTs deplete B cells efficiently and alter the B cell phenotype after reconstitution

(A) UMAP of 52,500 cells randomly sampled from the combined dataset. The number of sampled cells was constant across samples. Color code indicates the main clusters generated through clustering and manual annotation.

(B) Heatmap showing the median marker expression across the identified main clusters defined from the combined dataset signature including all samples.

(C) Heatmap shows the median marker expression across the identified B cell subclusters.

(D) Frequency of B cell subsets among total cells across time after infusion. Points represent individual PBMC samples (n = 36). The line represents the conditional mean of B cell subset frequency.

(E and F) Untreated/treated PBMC samples of 8 patients with MS, resulting in 16 samples (before and after treatment).

(E) Pie chart showing the composition of distinct subsets within the B cell compartment before (left) and after (right) treatment. The after-treatment B cell compartment consists of late time points representing the replenishing B cell compartment. For after-treatment time points, samples with the highest B cell frequency were selected, and a 100-B cell threshold was applied, only including patients who qualified for both before and after treatment time points (n = 8 patients).

(F) Violin plots showing longitudinal changes in the frequency across B cell subsets in BCDT-treated MS (n = 8 patients; n = 16 samples). Paired Wilcoxon rank-sum test and Benjamini-Hochberg correction were applied.

association with MS susceptibility, particularly those encoding for class II MHC molecules.[22–25]

The characterization of the replenished B cell population after depletion with BCDTs has been examined before,[14,16,19] but studies investigating the immune compartment as a whole are missing. Here, we systematically investigated the effects of BCDTs on the peripheral immune landscape in patients with MS. We used high-dimensional mass cytometry in conjunction with unsupervised clustering to analyze the systemic immune compartment of patients with MS after BCDTs in a longitudinal manner. B cell depletion evoked alterations in CD4⁺ T cell composition and expression of co-stimulatory molecules, suggesting that the cell-to-cell interactions between B and T cells play a key role during MS immunopathology that could be compromised using BCDTs. Our study thereby addresses the enigmatic role of B cells in MS pathology and suggests a co-stimulatory mechanism of action for B cell-depleting agents in patients with MS.

RESULTS

Composition of the replenishing B cell compartment is altered

To characterize the immune landscape of patients with MS after BCDT, we collected longitudinal peripheral blood mononuclear cell (PBMC) samples of patients with MS undergoing BCDT (Table S1). As the pool of available patients was restricted (n = 12), we combined patients treated with ocrelizumab and rituximab, both of which target CD20 and exhibit comparable mechanisms of action.[26] The samples were analyzed by two partially overlapping mass cytometry panels in order to deeply interrogate cellular states and subsets associated with the clinical success of BCDT. Dimensionality reduction using uniform manifold approximation and projection (UMAP) and unsupervised FlowSOM clustering identified B cells, CD4⁺ T cells, CD8⁺ T cells, regulatory T (Treg) cells, γδ
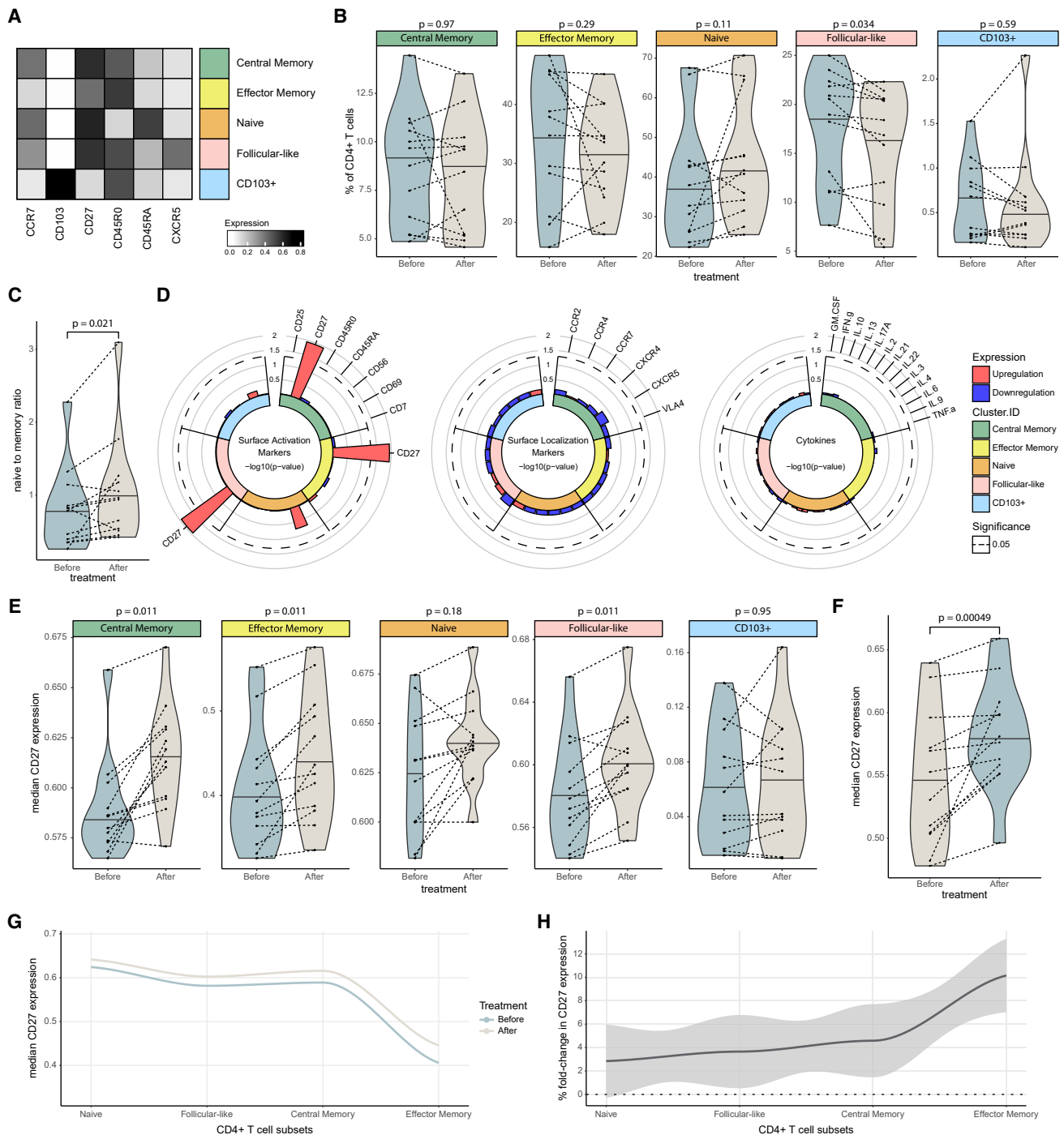
Figure 2. BCDTs alter the peripheral CD4⁺ T cell landscape of patients with MS

(A) Heatmap showing median expression of lineage markers across identified CD4⁺ T cell subsets defined from the combined dataset signature including all samples.

(B–F) Untreated/treated PBMC samples of 12 patients with MS, resulting in 24 samples (before and after treatment) analyzed longitudinally.

(B) Violin plots showing changes in the frequency across CD4⁺ T cell subsets in BCDT-treated MS. Paired Wilcoxon rank-sum test and Benjamini-Hochberg correction were applied.

(C) Violin plot showing changes in the naïve-to-memory ratio within the CD4⁺ T cell compartment. Paired Wilcoxon rank-sum test was applied.

(D) Radar plots showing changes in the marker expression of CD4⁺ T cell subsets in BCDT-treated MS. Values correspond to −log10(p value) and were adjusted with the Benjamini-Hochberg correction. Inner circle color annotations denote each respective subset. Bar color denotes the upregulation or downregulation of the respective marker. Marker order is consistent across subsets. Dashed line denotes −log10(0.05) cutoff for p value.

(legend continued on next page)

T cells, natural killer (NK) cells, and myeloid cells (Figures 1A and 1B).

To assess the kinetics of the impact of BCDTs on discrete B cell subsets, B cells were dissected into canonical B cell subsets: memory, naive, marginal zone-like (MZ-like), and plasmablasts (Figures 1C and S1A). In line with previous reports,[27] each of the investigated B cell subsets was efficiently depleted after treatment infusions (Figure 1D). To assess how the newly repopulating B cell compartment differed following BCDT, we compared, for each patient, the B cell composition before therapy initiation to a specific time point where a partial replenishment could be observed (time points ranging from 8 to 45 weeks since last infusion, median 22; 106–7,041 cell counts, median 399). Consistent with previous reports in the literature,[28] we observed a decrease in the frequency of memory B cells and an increase in the frequency of naive B cells (Figures 1E and 1F).

B cell depletion reduces the frequency of T follicular helper-like cells in patients with MS

To have a broad overview of the impact of BCDTs on the immune compartment, we investigated the frequency of distinct immune cell populations in patients with MS before and after therapy. To account for the bias elicited by the depletion of B cells, we computationally removed them from our analysis and normalized the frequencies accordingly. No significant changes were observed in the frequencies of canonical immune cell populations, which led us to conclude that further detailed analyses were necessary (Figure S1B).

B and T cell interactions have a fundamental role during the immunopathology of MS,[29] and interference with these interactions could partially account for the clinical efficacy of BCDTs. To better characterize the impact of BCDTs on the T cell compartment, we defined five distinct CD4$^+$ T cell subsets in the peripheral blood of patients with MS; central memory, effector memory, naive, T follicular helper-like (Tfh-like), and CD103$^+$ cells (Figure 2A). For each subset, we longitudinally analyzed the shift in the frequency after BCDT (Figure 2B). We observed a significant decrease in the frequency of Tfh-like cells in response to BCDT treatment. Circulating Tfh-like cells have been reported to be increased not only in the blood but also in the cerebrospinal fluid (CSF) of patients with MS, with a decrease in their blood levels being associated with a remission of the disease.[30–32]

These observations suggest that BCDTs may indirectly deplete potentially pathogenic Tfh-like cells and highlight the interdependence of these with B cells. Consistent with previous observations,[33] when comparing changes in the naive-to-memory ratio, we observed a shift from memory toward naive T helper (Th) cells (Figure 2C).

Analogous to the CD4$^+$ T cell compartment, we defined distinct subsets within the CD8$^+$ T cell compartment (Figure S2A). Analyzing the shift in the frequency of these subsets in BCDT-treated patients with MS, we observed that these were largely unaffected in response to BCDT treatment (Figure S2B). Accordingly, the ratio of naive-to-memory cytotoxic T cells was unchanged between untreated and treated patients with MS (Figure S2C). Despite the dominance of CD8$^+$ T cells over CD4$^+$ T cells in lesions of patients with MS and their potential involvement in the immunopathology of MS,[34–36] these results point toward a highly selective influence of BCDTs on the Th cell compartment.

B cell depletion leads to selective increase in CD27 expression across memory Th cell subsets

Next, we assessed whether phenotypic alterations in CD4$^+$ T cell subsets could be associated with BCDTs. To accomplish this, we assigned each marker to one of three mutually exclusive groups: surface activation markers, surface localization markers, and cytokines. We then examined how the expression levels of each subset changed in response to B cell depletion over time and found a selective disparity in CD27 expression in Th cell subsets, with increased surface CD27 across central and effector memory Th cells as well as Tfh-like cells (Figures 2D and 2E). This upregulation of CD27 was also consistently observed in the Th cell compartment as a whole, indicating that the effect is persistent (Figure 2F). Interestingly, soluble CD27 (sCD27) in the CSF is a prognostic biomarker in MS, and its protein levels are directly correlated with disease severity.[37–39]

The co-stimulatory molecule CD27 is part of the tumor necrosis factor receptor superfamily (TNFRSF), and its ligand CD70 is expressed by APCs.[40–43] CD27 signaling leads to the induction of pro-survival pathways[44,45] and supports the efficient expansion and differentiation of activated T cells.[46–49] CD27 expression is transiently upregulated upon T cell receptor (TCR) engagement[50–52] and proteolytically cleaved and released as sCD27 upon sustained signaling.[37,53,54] Surface expression of CD27 therefore naturally declines along the T cell differentiation path,[42] with naive T cells having the highest expression and more differentiated subsets showing a lower expression. Thus, higher surface CD27 expression levels may be a result of impaired interaction due to the depletion of CD70-expressing B cells and could represent an attenuation of CD27 signaling. Indeed, when we examined surface CD27 levels along the differentiation path of Th cells, we observed an overall increased expression after BCDT (Figure 2G). This effect was most pronounced in more differentiated Th cell subsets (Figure 2H). In summary, the heightened surface expression of CD27 is likely a result of diminished interaction with CD70 on B cells. The interplay between B and Th cells may contribute to the disease progression in MS, and this process could be disrupted by the action of BCDTs.

Next, we assessed changes in marker expression in the CD8$^+$ T cell compartment analogous to the previous analysis for the CD4$^+$ T cells. Notably, we observed a downregulation of surface

---

(E) Violin plots showing changes in CD27 expression across CD4$^+$ T cell subsets in BCDT-treated MS. p values correspond to the paired Wilcoxon rank-sum test applying a Benjamini-Hochberg correction.

(F) Violin plot showing changes in CD27 expression in the CD4$^+$ T cell compartment in BCDT-treated MS. Paired Wilcoxon rank-sum test was applied.

(G) Median CD27 expression along CD4$^+$ T cell subsets of the patients with MS. Color code denotes patient values before or after treatment.

(H) Percentage of fold change in CD27 expression along CD4$^+$ T cell subsets of the patients with MS, depicted in percentage of changes. Shaded area represents the 95% confidence interval.
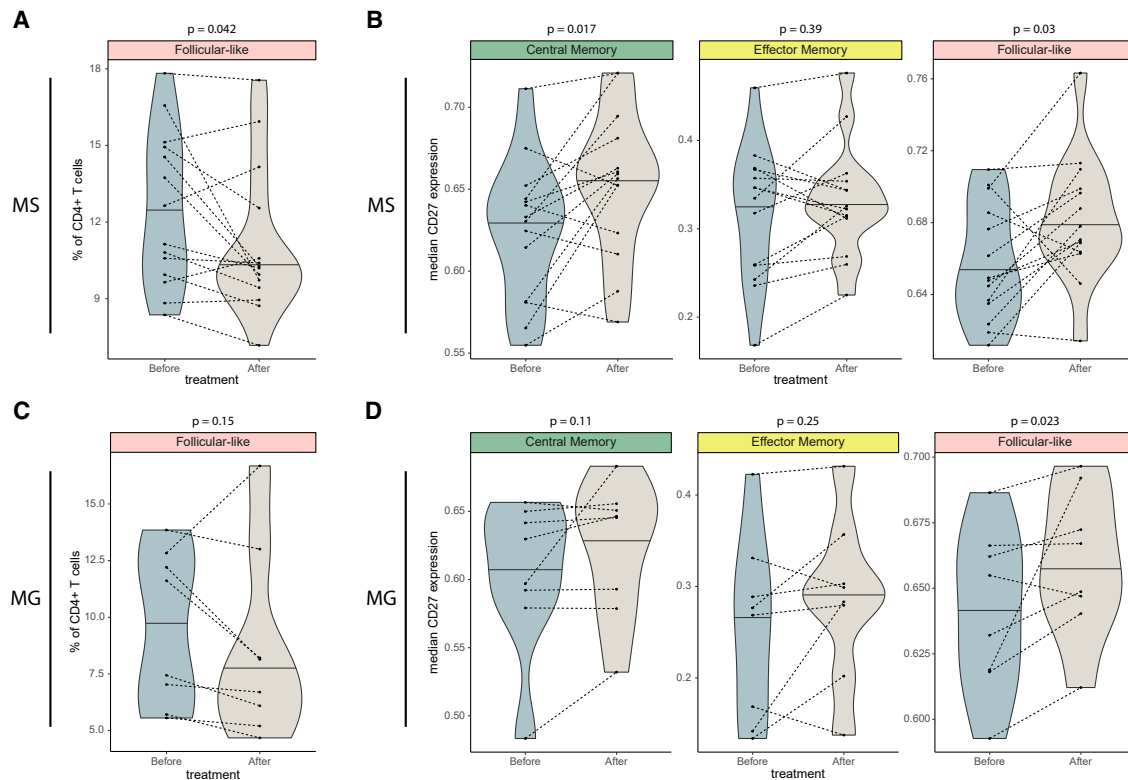
Figure 3. The altered CD4⁺ T cell landscape is consistent across cohorts

(A and B) Untreated/treated PBMC samples of 14 patients with MS, resulting in 28 samples (before and after treatment) analyzed longitudinally.

(A) Violin plot showing the frequency in CD4⁺ Tfh-like cells in B cell-depleted patients with MS of the validation cohort. Paired Wilcoxon rank-sum test was applied.

(B) Violin plots showing changes in CD27 expression across CD4⁺ memory and Tfh-like cells in B cell-depleted patients with MS of the validation cohort. Paired Wilcoxon rank-sum test was applied.

(C and D) Untreated/treated PBMC samples of 8 patients with MG, resulting in 16 samples (before and after treatment) analyzed longitudinally.

(C) Violin plot showing the frequency in CD4⁺ Tfh-like cells in B cell-depleted patients with MG of the validation cohort. Paired Wilcoxon rank-sum test was applied.

(D) Violin plots showing changes in CD27 expression across CD4⁺ memory and Tfh-like cells in B cell-depleted patients with MG of the validation cohort. Paired Wilcoxon rank-sum test was applied.

CXCR4 in effector memory, effector, and NKT-like T cells (Figures S2D and S2E). It is worth mentioning that increased CXCR4 expression within PBMCs has been reported in the context of MS and has been suggested as a potential biomarker.[55] Furthermore, we also noted a downregulation in surface CXCR5 within effector memory cells (Figure S2D). However, given the extremely low abundance of CXCR5 and the mild changes after BCDTs, it is unlikely that this observation carries much biological significance (Figure S2F). CD27 expression levels during cytotoxic T cell differentiation followed a similar surface expression pattern to that observed for the CD4⁺ T cell counterpart but did not reveal any changes as a result of BCDT, highlighting the selectivity of BCDT on the Th cell compartment (Figures S2G and S2H).

Independent cohort analysis confirmed impact of BCDTs on the Th cell compartment

Using an independent cohort from a distinct clinical center (Table S2), we sought to validate the selective effects of BCDTs on the Th cell compartment. Consistent with the analysis of the discovery cohort, we observed a reduction in circulating Tfh-like cells after BCDT (Figure 3A). Furthermore, when analyzing changes in CD27 expression across CD4⁺ memory T cell and Tfh-like cell subsets, we replicated our findings for the central memory Th cells and Tfh-like cells but not for the effector memory Th cells (Figure 3B). In conclusion, using a separate cohort of BCDT-treated patients with MS, we confirmed the decrease in Tfh-like cell frequency and the increase in surface expression of CD27 across select Th cell subsets as a quantifiable effect of the therapy.

BCDT in patients with myasthenia gravis induced CD27 expression in Tfh-like cells

To assess whether the selective influence of BCDTs on the Th cell compartment was specific to MS pathophysiology or a universal feature of BCDTs, we next analyzed the influence of BCDTs on the CD4⁺ T cell compartment in patients with myasthenia gravis (MG) in an independent cohort (Table S3). The patients were selected to be treatment naive to immune suppressants except for exposure to low to moderate doses of corticosteroids in some cases. Longitudinal comparison of Tfh-like cell frequencies
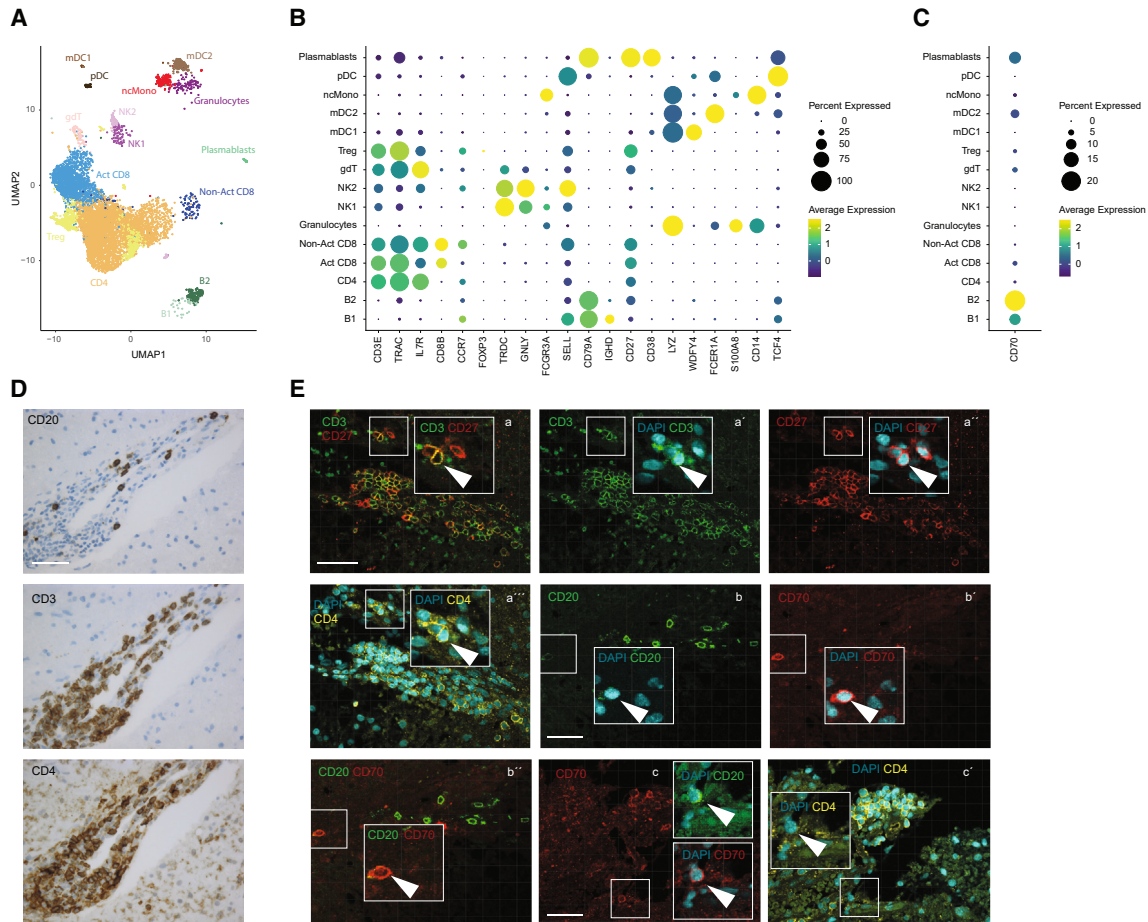
Figure 4. CD70 expression in CNS of patients with MS

(A–C) Single-cell RNA sequencing data from Schafflick et al. derived from the CSF of patients with MS.

(A) UMAP displaying the cellular composition of the CSF in MS. The color code corresponds to the clusters as defined in the study.

(B) Dot plot illustrating specific marker genes across distinct clusters. Dot size correlates with the percentage of cells within each cluster expressing the chosen marker, while the color code represents the average marker expression level within the respective cluster.

(C) Dot plot illustrating CD70 gene across distinct clusters. Dot size correlates with the percentage of cells within each cluster expressing CD70, while the color code represents the average CD70 expression level within the respective cluster.

(D and E) Brain tissue from a patient with relapsing MS with tumefactive brain lesions (n = 3 formalin-fixed, paraffin-embedded brain biopsy samples were examined).

(D) Representative immunostaining of CD20+ B cells and CD4+ CD3+ T cells in proximity in inflammatory MS lesions. Scale bar, 20 μm.

(E) Representative immunofluorescence (IF) images of CD27-expressing CD4+ CD3+ T cells (a–a‴) and CD70-expressing CD20+ B cells in or close to inflammatory infiltrates in MS brain biopsies (b–b″, c, and c′). Insets show enlargement of areas outlined in main images. Arrowheads show co-localization; nuclear DAPI staining in blue. Image labels (a), (b), and (c) denote distinct brain lesion sites of the representative patient with MS. Scale bars, 40 μm.

revealed a decreasing trend (Figure 3C). Equally, when we evaluated the surface CD27 expression across memory T cells and Tfh-like cells in response to BCDTs, we observed a trend toward upregulation (Figure 3D). However, we found a significant increase in CD27 expression specifically in Tfh-like cells. Despite the disparity in clinical efficacy of BCDTs in MS and MG,[56,57] we can conclude that upregulation of CD27 in Tfh-like cells is a universal hallmark of the therapy.

Human MS lesions contain CD27+ CD4+ T cells and CD70-expressing B cells

Our findings suggested a mechanism of action of BCDTs leading to decreased interaction between CD27+ Th cells and CD70+ B cells. To substantiate this notion, we analyzed publicly available single-cell RNA sequencing data from CSF of patients with MS as previously reported by Schafflick et al.[32] We adopted the clustering methodology described in the original study, with a specific focus on the CSF dataset (Figures 4A and 4B).

Upon examining CD70 expression levels across the identified clusters, we observed the highest expression, coupled with the highest proportion of CD70+ cells, within conventional B cells (B2) (Figure 4C). Notably, it is well established that surface CD27 on Th cells predominantly interacts with CD70 expressed by professional APCs.[41] In our analysis, CD70 expression was significantly elevated in conventional B cells compared to other

APCs, including plasmacytoid dendritic cells (pDCs) and myeloid DCs (mDCs) type I and II.

To further test the presence of CD27^{+} CD4^{+} T cells and CD70^{+} B cells within inflammatory lesions in human MS brain parenchyma, we stained biopsy sections of 3 patients with relapsing-remitting MS by immunohistochemistry. We observed the co-localization of CD4^{+} CD3^{+} T cells and, to a lesser extent, CD20^{+} B cells within lesion sites (Figure 4D). Furthermore, CD27-expressing CD4^{+} CD3^{+} T cells (Figure 4E, a–a‴) and a smaller proportion of CD70-expressing CD20^{+} B cells co-inhabited the same lesion sites (Figure 4E, b–b″, c, and c′). While most Th (CD4^{+}/CD3^{+}) cells, accumulating at lesions, stained positive for CD27 to a variable degree, we could also detect a few non-T cells that expressed CD27 (Figure 4E, a–a‴). In accordance with the literature and the publicly available MS CSF data, CD70 was expressed by a subset of CD20^{+} B cells in MS lesions, and CD70 could also be found on a small proportion of T cells (Figure 4E, b–b″, c, and c′).

Collectively, our findings strongly support the scenario that the CD27/CD70 interactions within the inflamed brain parenchyma primarily occur between Th cells and B cells.

DISCUSSION

BCDT is one of the most impactful therapeutic advancements for the treatment of MS to date.[7] Nevertheless, the mechanism by which BCDTs mediate their clinical efficacy remains largely unknown. As mentioned above, the cardinal feature of B cells, namely the production of antibodies, cannot be responsible for the effect in MS. Nonetheless, it is intriguing that the mechanism by which BCDT exerts its effect on disease progression remains incompletely understood.

We have recently discovered that the systemic immune profile of individuals with MS, when compared to healthy individuals, only slightly differs in its signature.[58] Another recent study demonstrated subtle modifications within the CD8^{+} T cell population in patients undergoing BCDT treatment.[59] Considering that B cell depletion effectively removes 5%–10% lymphocytes from the PBMC compartment, the subtlety of the consequences for the remaining immune compartment is rather surprising. When considering genetic variations while examining monozygotic twin pairs discordant for MS, minimal disparities were detected in the frequencies of canonical leukocytes.[60] As a result, longitudinal samples that also consider genetic susceptibility yield superior signal-to-noise ratios. These cohorts have facilitated the discovery of potential biomarkers for treatment responses, such as in patients undergoing oral MS therapy with dimethyl fumarate.[61,62]

In this study, we sought to provide an unbiased roadmap of the systemic immune compartment in response to the elimination of B cells. To better understand how BCDT alters the non-B cell immune compartment, we designed an immunophenotyping protocol combined with a comprehensive algorithm-guided analysis. Our extensive statistical analyses, backed by replicating our results using an independent validation cohort, provided reliable insights of the effects of BCDTs in MS.

We demonstrated a highly selective influence of BCDTs on the CD4^{+} T cell compartment in the peripheral blood of patients with MS. Particularly, we observed an upregulation of surface CD27 levels along the Th cell differentiation path in response to BCDTs that was most pronounced in memory Th cells and Tfh-like cells. Upon sustained signaling, CD27 is cleaved into its soluble form. Thus, the observed upregulation of CD27 in response to BCDTs suggests a potential attenuation of the CD27/CD70 signaling pathway.

Leveraging publicly available single-cell RNA sequencing data, we confirmed, in line with previous reports,[63] that B cells have the highest expression of CD70 within the CSF of patients with MS. Moreover, we demonstrated the co-localization of CD70-expressing B cells and CD27-expressing Th cells to CNS lesion sites. Together, our findings suggest that dysregulated interactions between B and Th cells may play an important role in driving the pathogenesis of MS and that the effectiveness of BCDTs could partially hinge on the disruption of these interactions. As loss of surface CD27 is a recognized molecular feature of terminal differentiation,[51,64] disruption of these interactions by BCDTs could lead to an impediment in the activity of Th cells, partially contributing to the efficacy of the therapies.

In line with the proposed mechanism of action, elevated levels of sCD27 in the CSF have been well established as a biomarker for MS[37] and have shown a positive correlation with relapse rates.[65] Similarly, sCD27 levels in the CSF of patients with MS have proven to be highly predictive of active intrathecal inflammation.[38] Decreased sCD27 levels in the CSF have been observed in response to common MS therapies, including BCDTs.[66–68] Further evidence supporting the involvement of the CD27/CD70 pathway in MS comes from studies utilizing preclinical models of the disease. These studies have demonstrated that administration of an anti-CD70 monoclonal antibody significantly suppressed experimental autoimmune encephalomyelitis (EAE) and Theiler's murine encephalomyelitis virus-induced demyelinating disease (TMEV-IDD), resulting in reduced clinical scores, inflammation, and demyelination levels.[69,70] Similarly, in a transgenic mouse model where the TCR recognizes the myelin oligodendrocyte glycoprotein, constitutive CD70 expression on B cells increased the susceptibility of mice toward spontaneous EAE development.[71]

In addition to a dysregulation in the B cell/T cell interface via the CD27/CD70 axis, we observed a significant decrease in the frequency of Tfh-like cells in patients with MS after treatment with BCDTs. Given the central role of Tfh-like cells in providing co-stimulatory maturation and proliferation signals to B cells, their decrease in frequency after depletion of B cells highlights the importance of direct cell-cell interactions during the immunopathology of MS. Numerous studies underscore the importance of Tfh-like cells in MS pathophysiology.[30–32,72] CXCL13, a chemokine involved in the migration of B cells and Tfh-like cells,[73,74] is found to be elevated in the CSF of patients with MS[75] and is predictive of a more severe disease course.[76] Furthermore, rituximab treatment has been shown to decrease CXCL13 as well as T cells in the CSF in a proportional manner.[77] CXCL13 is prominently produced by actively demyelinating lesions but not by chronic inactive lesions.[78–80] Finally, increased levels of circulating as well as CSF Tfh-like cells have been reported in MS and found to be reduced in patients with complete remission.[30–32]

In conclusion, our study highlights the specific impact of BCDTs on the Th cell compartment in individuals with MS. These findings suggest that the interplay between B and Th cells may play a significant role in the progression of MS, and the effectiveness of BCDTs in treating the disease may be partly attributed to the disruption of these interactions through B cell depletion. Importantly, further investigation into the involvement of the CD27/CD70 pathway in B and T cell interactions shows promise and is warranted. Our findings establish a connection between the prognostic marker sCD27 and the mechanism of action of BCDTs, shedding light on the pathophysiology of MS and offering potential insights into the clinical efficacy of BCDTs. Additionally, our analysis reports a significant reduction in the frequency of Tfh-like cells in response to the therapy and emphasizes their involvement in MS as suggested by others.

Limitations of the study

It was vital for this study to include patients treated with BCDT and to obtain samples prior to as well as after the treatment induction. This fact is mainly responsible for the relatively limited sample size and therefore limited statistical power. Nevertheless, our findings could be validated in patient cohorts obtained from two independent clinical centers. Current untargeted single-cell technologies (e.g., RNA sequencing [RNA-seq]) are limited in their throughput and resolution, but they could have potentially revealed additional alterations driven by BCDT. As a compromise, here, we used CyTOF, which allowed for a combined analysis of multiple barcoded patient samples. Even though the dynamic range for detection of protein expression and reproducibility across the samples is very good, the quasi-targeted nature of CyTOF may create a bias. Finally, this study would have benefitted from access to longitudinal CSF samples, which likely are more reflective of the events that occur within inflammatory CNS lesions. However, it is important to note that lumbar puncture of patients with MS is typically only performed diagnostically and that obtaining CSF samples from these patients after treatment is often not possible.

STAR★METHODS

Detailed methods are provided in the online version of this paper and include the following:

- KEY RESOURCES TABLE
- RESOURCE AVAILABILITY
  - Lead contact
  - Materials availability
  - Data and code availability
- EXPERIMENTAL MODEL AND STUDY PARTICIPANT DETAILS
  - Longitudinal PBMC samples of MS patients during BCDT in the discovery cohort
  - Longitudinal PBMC samples of MS and MG patients during BCDT in the validation cohort
  - Histology samples
- METHOD DETAILS
  - *Ex vivo* activation of PBMCs from MS patients
  - Live cell barcoding for mass cytometry
  - Surface and intracellular cytokine staining for mass cytometry
  - Mass cytometry data acquisition and preprocessing
  - Batch normalization
  - High-dimensional analysis
  - Immunostaining of human brain tissue
- QUANTIFICATION AND STATISTICAL ANALYSIS

REFERENCES

1. Bar-Or, A. (2008). The Immunology of Multiple Sclerosis. Semin. Neurol. *28*, 29–45.

2. Dendrou, C.A., Fugger, L., and Friese, M.A. (2015). Immunopathology of multiple sclerosis. Nat. Rev. Immunol. *15*, 545–558.

3. van Oosten, B.W., Lai, M., Hodgkinson, S., Barkhof, F., Miller, D.H., Moseley, I.F., Thompson, A.J., Rudge, P., McDougall, A., McLeod, J.G., et al. (1997). Treatment of multiple sclerosis with the monoclonal anti-CD4 antibody cM-T412: Results of a randomized, double-blind, placebo-controlled MR-monitored phase II trial. Neurology *49*, 351–357.

4. Gelfand, J.M., Cree, B.A.C., and Hauser, S.L. (2017). Ocrelizumab and Other CD20+ B-Cell-Depleting Therapies in Multiple Sclerosis. Neurotherapeutics *14*, 835–841.

5. Li, R., Patterson, K.R., and Bar-Or, A. (2018). Reassessing B cell contributions in multiple sclerosis. Nat. Immunol. *19*, 696–707.

6. Hauser, S.L., Waubant, E., Arnold, D.L., Vollmer, T., Antel, J., Fox, R.J., Bar-Or, A., Panzara, M., Sarkar, N., Agarwal, S., et al. (2008). B-Cell Depletion with Rituximab in Relapsing–Remitting Multiple Sclerosis. N. Engl. J. Med. *358*, 676–688.

7. Comi, G., Bar-Or, A., Lassmann, H., Uccelli, A., Hartung, H.-P., Montalban, X., Sørensen, P.S., Hohlfeld, R., and Hauser, S.L.; Expert Panel of the 27th Annual Meeting of the European Charcot Foundation (2021). Role of B Cells in Multiple Sclerosis and Related Disorders. Ann. Neurol. *89*, 13–23.

8. Lee, D.S.W., Rojas, O.L., and Gommerman, J.L. (2021). B cell depletion therapies in autoimmune disease: advances and mechanistic insights. Nat. Rev. Drug Discov. *20*, 179–199.

9. Gordon, P.A., Carroll, D.J., Etches, W.S., Jeffrey, V., Marsh, L., Morrice, B.L., Olmstead, D., and Warren, K.G. (1985). A Double-blind Controlled Pilot Study of Plasma Exchange versus Sham Apheresis in Chronic Progressive Multiple Sclerosis. Can. J. Neurol. Sci. *12*, 39–44.

10. Weinshenker, B.G., O'Brien, P.C., Petterson, T.M., Noseworthy, J.H., Lucchinetti, C.F., Dodick, D.W., Pineda, A.A., Stevens, L.N., and Rodriguez, M. (1999). A randomized trial of plasma exchange in acute central nervous system inflammatory demyelinating disease. Ann. Neurol. *46*, 878–886.

11. Pöhlau, D., Przuntek, H., Sailer, M., Bethke, F., Koehler, J., König, N., Heesen, C., Späth, P., and Andresen, I. (2007). Intravenous immunoglobulin in primary and secondary chronic progressive multiple sclerosis: a randomized placebo controlled multicentre study. Mult. Scler. *13*, 1107–1117.

12. Fazekas, F., Lublin, F.D., Li, D., Freedman, M.S., Hartung, H.P., Rieckmann, P., Sørensen, P.S., Maas-Enriquez, M., Sommerauer, B., Hanna, K., et al. (2008). Intravenous immunoglobulin in relapsing-remitting multiple sclerosis: A dose-finding trial. Neurology *71*, 265–271.

13. Fazekas, F., Sørensen, P.S., Filippi, M., Ropele, S., Lin, X., Koelmel, H.W., Fernandez, O., Pozzilli, C., O'Connor, P., Enriquez, M.M., et al. (2005). MRI results from the European Study on Intravenous Immunoglobulin in Secondary Progressive Multiple Sclerosis (ESIMS). Mult. Scler. *11*, 433–440.

14. Duddy, M., Niino, M., Adatia, F., Hebert, S., Freedman, M., Atkins, H., Kim, H.J., and Bar-Or, A. (2007). Distinct Effector Cytokine Profiles of Memory and Naive Human B Cell Subsets and Implication in Multiple Sclerosis. J. Immunol. *178*, 6092–6099.

15. Bar-Or, A., Fawaz, L., Fan, B., Darlington, P.J., Rieger, A., Ghorayeb, C., Calabresi, P.A., Waubant, E., Hauser, S.L., Zhang, J., and Smith, C.H. (2010). Abnormal B-cell cytokine responses a trigger of T-cell–mediated disease in MS? Ann. Neurol. *67*, 452–461.

16. Barr, T.A., Shen, P., Brown, S., Lampropoulou, V., Roch, T., Lawrie, S., Fan, B., O'Connor, R.A., Anderton, S.M., Bar-Or, A., et al. (2012). B cell depletion therapy ameliorates autoimmune disease through ablation of IL-6–producing B cells. J. Exp. Med. *209*, 1001–1010.

17. Blanco-Jerez, C., Plaza, J.F., Masjuan, J., Orensanz, L.M., and Alvarez-Cermeño, J.C. (2002). Increased levels of IL-15 mRNA in relapsing–remitting multiple sclerosis attacks. J. Neuroimmunol. *128*, 90–94.

18. Rentzos, M., Cambouri, C., Rombos, A., Nikolaou, C., Anagnostouli, M., Tsoutsou, A., Dimitrakopoulos, A., Triantafyllou, N., and Vassilopoulos, D. (2006). IL-15 is elevated in serum and cerebrospinal fluid of patients with multiple sclerosis. J. Neurol. Sci. *241*, 25–29.

19. Li, R., Rezk, A., Miyazaki, Y., Hilgenberg, E., Touil, H., Shen, P., Moore, C.S., Michel, L., Althekair, F., Rajasekharan, S., et al. (2015). Proinflammatory GM-CSF–producing B cells in multiple sclerosis and B cell depletion therapy. Sci. Transl. Med. *7*, 310ra166.

20. Miyazaki, Y., Li, R., Rezk, A., Misirliyan, H., Moore, C., Farooqi, N., Solis, M., Goiry, L.G., de Faria Junior, O., Dang, V.D., et al. (2014). A Novel MicroRNA-132-Surtuin-1 Axis Underlies Aberrant B-cell Cytokine Regulation in Patients with Relapsing-Remitting Multiple Sclerosis. PLoS One *9*, e105421.

21. Ghosh, D., Jiang, W., Mukhopadhyay, D., and Mellins, E.D. (2021). New insights into B cells as antigen presenting cells. Curr. Opin. Immunol. *70*, 129–137.

22. Lincoln, M.R., Montpetit, A., Cader, M.Z., Saarela, J., Dyment, D.A., Tiislar, M., Ferretti, V., Tienari, P.J., Sadovnick, A.D., Peltonen, L., et al. (2005). A predominant role for the HLA class II region in the association of the MHC region with multiple sclerosis. Nat. Genet. *37*, 1108–1112.

23. Olerup, O., and Hillert, J. (1991). HLA class II-associated genetic susceptibility in multiple sclerosis: A critical evaluation. Tissue Antigens *38*, 1–15.

24. Spurkland, A., Rønningen, K.S., Vandvik, B., Thorsby, E., and Vartdal, F. (1991). HLA-DQA1 and HLA-DQB1 genes may jointly determine susceptibility to develop multiple sclerosis. Hum. Immunol. *30*, 69–75.

25. Jersild, C., Fog, T., Hansen, G.S., Thomsen, M., Svejgaard, A., and Dupont, B. (1973). HISTOCOMPATIBILITY DETERMINANTS IN MULTIPLE SCLEROSIS, WITH SPECIAL REFERENCE TO CLINICAL COURSE. Lancet *2*, 1221–1225.

26. Alcalá, C., Quintanilla-Bordás, C., Gascón, F., Sempere, Á.P., Navarro, L., Carcelén-Gadea, M., Landete, L., Mallada, J., Cañizares, E., Belenguer, A., et al. (2022). Effectiveness of rituximab vs. ocrelizumab for the treatment of primary progressive multiple sclerosis: a real-world observational study. J. Neurol. *269*, 3676–3681.

27. Maloney, D.G., Grillo-López, A.J., Bodkin, D.J., White, C.A., Liles, T.M., Royston, I., Varns, C., Rosenberg, J., and Levy, R. (1997). IDEC-C2B8: results of a phase I multiple-dose trial in patients with relapsed non-Hodgkin's lymphoma. J. Clin. Oncol. *15*, 3266–3274.

28. Bar-Or, A., Calabresi, P.A.J., Arnold, D., Markowitz, C., Shafer, S., Kasper, L.H., Waubant, E., Gazda, S., Fox, R.J., Panzara, M., et al. (2008). Rituximab in relapsing-remitting multiple sclerosis: A 72-week, open-label, phase I trial. Ann. Neurol. *63*, 395–400.

29. van Langelaar, J., Rijvers, L., Smolders, J., and van Luijn, M.M. (2020). B and T Cells Driving Multiple Sclerosis: Identity, Mechanisms and Potential Triggers. Front. Immunol. *11*, 760.

30. Fan, X., Jin, T., Zhao, S., Liu, C., Han, J., Jiang, X., and Jiang, Y. (2015). Circulating CCR7+ICOS+ Memory T Follicular Helper Cells in Patients with Multiple Sclerosis. PLoS One *10*, e0134523.

31. Guo, J., Zhao, C., Wu, F., Tao, L., Zhang, C., Zhao, D., Yang, S., Jiang, D., Wang, J., Sun, Y., et al. (2018). T Follicular Helper-Like Cells Are Involved in the Pathogenesis of Experimental Autoimmune Encephalomyelitis. Front. Immunol. *9*, 944.

32. Schafflick, D., Xu, C.A., Hartlehnert, M., Cole, M., Schulte-Mecklenbeck, A., Lautwein, T., Wolbert, J., Heming, M., Meuth, S.G., Kuhlmann, T., et al. (2020). Integrated single cell analysis of blood and cerebrospinal fluid leukocytes in multiple sclerosis. Nat. Commun. *11*, 247.

33. Lovett-Racke, A.E., Gormley, M., Liu, Y., Yang, Y., Graham, C., Wray, S., Racke, M.K., Shubin, R., Twyman, C., Alvarez, E., et al. (2019). B cell depletion with ublituximab reshapes the T cell profile in multiple sclerosis patients. J. Neuroimmunol. *332*, 187–197.

34. Huseby, E.S., Huseby, P.G., Shah, S., Smith, R., and Stadinski, B.D. (2012). Pathogenic CD8 T Cells in Multiple Sclerosis and Its Experimental Models. Front. Immunol. *3*, 64.

35. Babbe, H., Roers, A., Waisman, A., Lassmann, H., Goebels, N., Hohlfeld, R., Friese, M., Schröder, R., Deckert, M., Schmidt, S., et al. (2000). Clonal Expansions of CD8+ T Cells Dominate the T Cell Infiltrate in Active Multiple Sclerosis Lesions as Shown by Micromanipulation and Single Cell Polymerase Chain Reaction. J. Exp. Med. *192*, 393–404.

36. Salou, M., Garcia, A., Michel, L., Gainche-Salmon, A., Loussouarn, D., Nicol, B., Guillot, F., Hulin, P., Nedellec, S., Baron, D., et al. (2015). Expanded CD8 T-cell sharing between periphery and CNS in multiple sclerosis. Ann. Clin. Transl. Neurol. *2*, 609–622.

37. Hintzen, R.Q., van Lier, R.A.W., Kuijpers, K.C., Baars, P.A., Schaasberg, W., Lucas, C.J., and Polman, C.H. (1991). Elevated levels of a soluble form of the T cell activation antigen CD27 in cerebrospinal fluid of multiple sclerosis patients. J. Neuroimmunol. *35*, 211–217.

38. Komori, M., Blake, A., Greenwood, M., Lin, Y.C., Kosa, P., Ghazali, D., Winokur, P., Natrajan, M., Wuest, S.C., Romm, E., et al. (2015). Cerebrospinal fluid markers reveal intrathecal inflammation in progressive multiple sclerosis. Ann. Neurol. 78, 3–20.

39. Wong, Y.Y.M., van der Vuurst de Vries, R.M., van Pelt, E.D., Ketelslegers, I.A., Melief, M.-J., Wierenga, A.F., Catsman-Berrevoets, C.E., Neuteboom, R.F., and Hintzen, R.Q. (2018). T-cell activation marker sCD27 is associated with clinically definite multiple sclerosis in childhood-acquired demyelinating syndromes. Mult. Scler. 24, 1715–1724.

40. Agematsu, K., Hokibara, S., Nagumo, H., and Komiyama, A. (2000). CD27: a memory B-cell marker. Immunol. Today 21, 204–206.

41. Han, B.K., Olsen, N.J., and Bottaro, A. (2016). The CD27–CD70 pathway and pathogenesis of autoimmune disease. Semin. Arthritis Rheum. 45, 496–501.

42. Lens, S.M., Tesselaar, K., van Oers, M.H., and van Lier, R.A. (1998). Control of lymphocyte function through CD27–CD70 interactions. Semin. Immunol. 10, 491–499.

43. Nolte, M.A., Van Olffen, R.W., Van Gisbergen, K.P.J.M., and Van Lier, R.A.W. (2009). Timing and tuning of CD27–CD70 interactions: the impact of signal strength in setting the balance between adaptive responses and immunopathology. Immunol. Rev. 229, 216–231.

44. Dolfi, D.V., Boesteanu, A.C., Petrovas, C., Xia, D., Butz, E.A., and Katsikis, P.D. (2008). Late Signals from CD27 Prevent Fas-Dependent Apoptosis of Primary CD8+ T Cells1. J. Immunol. 180, 2912–2921.

45. Peperzak, V., Veraar, E.A.M., Keller, A.M., Xiao, Y., and Borst, J. (2010). The Pim Kinase Pathway Contributes to Survival Signaling in Primed CD8+ T Cells upon CD27 Costimulation. J. Immunol. 185, 6670–6678.

46. Hendriks, J., Gravestein, L.A., Tesselaar, K., van Lier, R.A., Schumacher, T.N., and Borst, J. (2000). CD27 is required for generation and long-term maintenance of T cell immunity. Nat. Immunol. 1, 433–440.

47. Hendriks, J., Xiao, Y., and Borst, J. (2003). CD27 Promotes Survival of Activated T Cells and Complements CD28 in Generation and Establishment of the Effector T Cell Pool. J. Exp. Med. 198, 1369–1380.

48. Hintzen, R.Q., Lens, S.M., Lammers, K., Kuiper, H., Beckmann, M.P., and van Lier, R.A. (1995). Engagement of CD27 with its ligand CD70 provides a second signal for T cell activation. J. Immunol. 154, 2612–2623.

49. Oshima, H., Nakano, H., Nohara, C., Kobata, T., Nakajima, A., Jenkins, N.A., Gilbert, D.J., Copeland, N.G., Muto, T., Yagita, H., and Okumura, K. (1998). Characterization of murine CD70 by molecular cloning and mAb. Int. Immunol. 10, 517–526.

50. Gravestein, L.A., Nieland, J.D., Kruisbeek, A.M., and Borst, J. (1995). Novel mAbs reveal potent co-stimulatory activity of murine CD27. Int. Immunol. 7, 551–557.

51. Hintzen, R.Q., de Jong, R., Lens, S.M., and van Lier, R.A.W. (1994). CD27: marker and mediator of T-cell activation? Immunol. Today 15, 307–311.

52. van Lier, R.A., Borst, J., Vroom, T.M., Klein, H., Van Mourik, P., Zeijlemaker, W.P., and Melief, C.J. (1987). Tissue distribution and biochemical and functional properties of Tp55 (CD27), a novel T cell differentiation antigen. J. Immunol. 139, 1589–1596.

53. Kato, K., Chu, P., Takahashi, S., Hamada, H., and Kipps, T.J. (2007). Metalloprotease inhibitors block release of soluble CD27 and enhance the immune stimulatory activity of chronic lymphocytic leukemia cells. Exp. Hematol. 35, 434–442.

54. Loenen, W.A., de Vries, E., Gravestein, L.A., Hintzen, R.Q., Van Lier, R.A., and Borst, J. (1992). The CD27 membrane receptor, a lymphocyte-specific member of the nerve growth factor receptor family, gives rise to a soluble form by protein processing that does not involve receptor endocytosis. Eur. J. Immunol. 22, 447–455.

55. Chen, X., Hou, H., Qiao, H., Fan, H., Zhao, T., and Dong, M. (2021). Identification of blood-derived candidate gene markers and a new 7-gene diagnostic model for multiple sclerosis. Biol. Res. 54, 12.

56. Piehl, F., Eriksson-Dufva, A., Budzianowska, A., Feresiadou, A., Hansson, W., Hietala, M.A., Håkansson, I., Johansson, R., Jons, D., Kmezic, I., et al. (2022). Efficacy and Safety of Rituximab for New-Onset Generalized Myasthenia Gravis: The RINOMAX Randomized Clinical Trial. JAMA Neurol. 79, 1105–1112.

57. Nowak, R.J., Coffey, C.S., Goldstein, J.M., Dimachkie, M.M., Benatar, M., Kissel, J.T., Wolfe, G.I., Burns, T.M., Freimer, M.L., Nations, S., et al. (2021). Phase 2 Trial of Rituximab in Acetylcholine Receptor Antibody-Positive Generalized Myasthenia Gravis: The BeatMG Study. Neurology 98, e376–e389.

58. Galli, E., Hartmann, F.J., Schreiner, B., Ingelfinger, F., Arvaniti, E., Diebold, M., Mrdjen, D., van der Meer, F., Krieg, C., Nimer, F.A., et al. (2019). GM-CSF and CXCR4 define a T helper cell signature in multiple sclerosis. Nat. Med. 25, 1290–1300.

59. Mathias, A., Pantazou, V., Perriot, S., Canales, M., Jones, S., Oberholster, L., Moulin, M., Fenwick, C., Bernard-Valnet, R., Théaudin, M., et al. (2023). Ocrelizumab Impairs the Phenotype and Function of Memory CD8+ T Cells: A 1-Year Longitudinal Study in Patients With Multiple Sclerosis. Neurol. Neuroimmunol. Neuroinflamm. 10, e200084.

60. Ingelfinger, F., Gerdes, L.A., Kavaka, V., Krishnarajah, S., Friebel, E., Galli, E., Zwicky, P., Furrer, R., Peukert, C., Dutertre, C.-A., et al. (2022). Twin study reveals non-heritable immune perturbations in multiple sclerosis. Nature 603, 152–158.

61. Diebold, M., Galli, E., Kopf, A., Sanderson, N., Callegari, I., Ingelfinger, F., Núñez, N.G., Benkert, P., Kappos, L., Kuhle, J., et al. (2022). Immunological Predictors of Dimethyl Fumarate-Induced Lymphopenia. Ann. Neurol. 91, 676–681.

62. Diebold, M., Galli, E., Kopf, A., Sanderson, N.S.R., Callegari, I., Benkert, P., Gonzalo Núñez, N., Ingelfinger, F., Herms, S., Cichon, S., et al. (2022). High-dimensional immune profiling identifies a biomarker to monitor dimethyl fumarate response in multiple sclerosis. Proc. Natl. Acad. Sci. USA 119, e2205042119.

63. Ramesh, A., Schubert, R.D., Greenfield, A.L., Dandekar, R., Loudermilk, R., Sabatino, J.J., Koelzer, M.T., Tran, E.B., Koshal, K., Kim, K., et al. (2020). A pathogenic and clonally expanded B cell transcriptome in active multiple sclerosis. Proc. Natl. Acad. Sci. USA 117, 22932–22943.

64. Hamann, D., Baars, P.A., Rep, M.H., Hooibrink, B., Kerkhof-Garde, S.R., Klein, M.R., and van Lier, R.A. (1997). Phenotypic and Functional Separation of Memory and Effector Human CD8+ T Cells. J. Exp. Med. 186, 1407–1418.

65. van der Vuurst de Vries, R.M., Mescheriakova, J.Y., Runia, T.F., Jafari, N., Siepman, T.A.M., and Hintzen, R.Q. (2017). Soluble CD27 Levels in Cerebrospinal Fluid as a Prognostic Biomarker in Clinically Isolated Syndrome. JAMA Neurol. 74, 286–292.

66. Komori, M., Lin, Y.C., Cortese, I., Blake, A., Ohayon, J., Cherup, J., Maric, D., Kosa, P., Wu, T., and Bielekova, B. (2016). Insufficient disease inhibition by intrathecal rituximab in progressive multiple sclerosis. Ann. Clin. Transl. Neurol. 3, 166–179.

67. Romme Christensen, J., Komori, M., von Essen, M.R., Ratzer, R., Börnsen, L., Bielekova, B., and Sellebjerg, F. (2019). CSF inflammatory biomarkers responsive to treatment in progressive multiple sclerosis capture residual inflammation associated with axonal damage. Mult. Scler. 25, 937–946.

68. Mahler, M.R., Søndergaard, H.B., Buhelt, S., von Essen, M.R., Romme Christensen, J., Enevold, C., and Sellebjerg, F. (2020). Multiplex assessment of cerebrospinal fluid biomarkers in multiple sclerosis. Mult. Scler. Relat. Disord. 45, 102391.

69. Nakajima, A., Oshima, H., Nohara, C., Morimoto, S., Yoshino, S., Kobata, T., Yagita, H., and Okumura, K. (2000). Involvement of CD70–CD27 interactions in the induction of experimental autoimmune encephalomyelitis. J. Neuroimmunol. 109, 188–196.

70. Yanagisawa, S., Takeichi, N., Kaneyama, T., Yagita, H., Taniguchi, S., Kim, B.S., and Koh, C.-S. (2010). Effects of anti-CD70 mAb on Theiler's murine encephalomyelitis virus-induced demyelinaiting disease. Brain Res. 1317, 236–245.

71. FrancoSalinas, G., Cantaert, T., Nolte, M.A., Tak, P.P., van Lier, R.A.W., and Baeten, D.L. (2013). Enhanced costimulation by CD70+ B cells aggravates experimental autoimmune encephalomyelitis in autoimmune mice. J. Neuroimmunol. *255*, 8–17.

72. Zhang, X., Ge, R., Chen, H., Ahiafor, M., Liu, B., Chen, J., and Fan, X. (2021). Follicular Helper CD4+ T Cells, Follicular Regulatory CD4+ T Cells, and Inducible Costimulator and Their Roles in Multiple Sclerosis and Experimental Autoimmune Encephalomyelitis. Mediators Inflamm. *2021*, 2058964.

73. Legler, D.F., Loetscher, M., Roos, R.S., Clark-Lewis, I., Baggiolini, M., and Moser, B. (1998). B Cell–attracting Chemokine 1, a Human CXC Chemokine Expressed in Lymphoid Tissues, Selectively Attracts B Lymphocytes via BLR1/CXCR5. J. Exp. Med. *187*, 655–660.

74. Ebert, L.M., Schaerli, P., and Moser, B. (2005). Chemokine-mediated control of T cell traffic in lymphoid and peripheral tissues. Mol. Immunol. *42*, 799–809.

75. Sellebjerg, F., Börnsen, L., Khademi, M., Krakauer, M., Olsson, T., Frederiksen, J.L., and Sørensen, P.S. (2009). Increased cerebrospinal fluid concentrations of the chemokine CXCL13 in active MS. Neurology *73*, 2003–2010.

76. Khademi, M., Kockum, I., Andersson, M.L., Iacobaeus, E., Brundin, L., Sellebjerg, F., Hillert, J., Piehl, F., and Olsson, T. (2011). Cerebrospinal fluid CXCL13 in multiple sclerosis: a suggestive prognostic marker for the disease course. Mult. Scler. *17*, 335–343.

77. Piccio, L., Naismith, R.T., Trinkaus, K., Klein, R.S., Parks, B.J., Lyons, J.A., and Cross, A.H. (2010). Changes in B- and T-Lymphocyte and Chemokine Levels With Rituximab Treatment in Multiple Sclerosis. Arch. Neurol. *67*, 707–714.

78. Corcione, A., Casazza, S., Ferretti, E., Giunti, D., Zappia, E., Pistorio, A., Gambini, C., Mancardi, G.L., Uccelli, A., and Pistoia, V. (2004). Recapitulation of B cell differentiation in the central nervous system of patients with multiple sclerosis. Proc. Natl. Acad. Sci. USA *101*, 11064–11069.

79. Krumbholz, M., Theil, D., Cepok, S., Hemmer, B., Kivisäkk, P., Ransohoff, R.M., Hofbauer, M., Farina, C., Derfuss, T., Hartle, C., et al. (2006). Chemokines in multiple sclerosis: CXCL12 and CXCL13 up-regulation is differentially linked to CNS immune cell recruitment. Brain *129*, 200–211.

80. Schmitt, N. (2015). Role of T Follicular Helper cells in Multiple Sclerosis. J. Nat. Sci. *1*, e139.

81. Van Gassen, S., Gaudilliere, B., Angst, M.S., Saeys, Y., and Aghaeepour, N. (2020). CytoNorm: A Normalization Algorithm for Cytometry Data. Cytometry A. *97*, 268–278.

82. Van Gassen, S., Callebaut, B., Van Helden, M.J., Lambrecht, B.N., Demeester, P., Dhaene, T., and Saeys, Y. (2015). FlowSOM: Using self-organizing maps for visualization and interpretation of cytometry data. Cytometry A. *87*, 636–645.

83. Wilkerson, M.D., and Hayes, D.N. (2010). ConsensusClusterPlus: a class discovery tool with confidence assessments and item tracking. Bioinformatics *26*, 1572–1573.

84. McInnes, L., Healy, J., Saul, N., and Großberger, L. (2018). UMAP: Uniform Manifold Approximation and Projection. J. Open Source Softw. *3*, 861.

85. Thompson, A.J., Banwell, B.L., Barkhof, F., Carroll, W.M., Coetzee, T., Comi, G., Correale, J., Fazekas, F., Filippi, M., Freedman, M.S., et al. (2018). Diagnosis of multiple sclerosis: 2017 revisions of the McDonald criteria. Lancet Neurol. *17*, 162–173.

86. Ingelfinger, F., Krishnarajah, S., Kramer, M., Utz, S.G., Galli, E., Lutz, M., Zwicky, P., Akarca, A.U., Jurado, N.P., Ulutekin, C., et al. (2021). Single-cell profiling of myasthenia gravis identifies a pathogenic T cell signature. Acta Neuropathol. *141*, 901–915.

87. Finck, R., Simonds, E.F., Jager, A., Krishnaswamy, S., Sachs, K., Fantl, W., Pe'er, D., Nolan, G.P., and Bendall, S.C. (2013). Normalization of mass cytometry data with bead standards. Cytometry A. *83*, 483–494.

88. Brummelman, J., Haftmann, C., Núñez, N.G., Alvisi, G., Mazza, E.M.C., Becher, B., and Lugli, E. (2019). Development, application and computational analysis of high-dimensional fluorescent antibody panels for single-cell flow cytometry. Nat. Protoc. *14*, 1946–1969.

STAR★METHODS

KEY RESOURCES TABLE

REAGENT or RESOURCE	SOURCE	IDENTIFIER
Antibodies		
Anti-human VLA4 (clone 9F10) (141 Pr)	Standard BioTools Inc	Cat# 3141004B; RRID: AB_2892684
Anti-human CCR6 (clone G034E3) (141 Pr)	Standard BioTools Inc	Cat# 3141003A; RRID: AB_2687639
Anti-human CD19 (clone HIB19) (142 Nd)	Standard BioTools Inc	Cat# 3142001B; RRID: AB_2651155
Anti-human CCR2 (clone K036C2) (purified)	Biolegend	Cat# 357202; RRID: AB_2561851
Anti-human IL-4 (clone MP4-25D2) (purified)	Biolegend	Cat# 500802; RRID: AB_315121
Anti-human CCR5 (clone J418F1) (purified)	Biolegend	Cat# 359101; RRID: AB_2562456
Anti-human CD4 (clone RPA-T4) (145 Nd)	Standard BioTools Inc	Cat# 3145001B; RRID: AB_2661789
Anti-human CD8 (clone RPA-T8) (146 Nd)	Standard BioTools Inc	Cat# 3146001B; RRID: AB_315088
Anti-human IL-2 (clone MQ1-17H12) (purified)	Biolegend	Cat# 500301; RRID: AB_2687641
Anti-human CD11c (clone BU15) (147 Sm)	Standard BioTools Inc	Cat# 3147008B; RRID: AB_2687850
Anti-human IL-17A (clone BL168) (148 Nd)	Standard BioTools Inc	Cat# 3148008B; RRID: N/A
Anti-human CD16 (clone 3G8) (148 Nd)	Standard BioTools Inc	Cat# 3148004B; RRID: AB_2661791
Anti-human IL-3 (clone BVD8-3G11) (purified)	Biolegend	Cat# 500502; RRID: AB_315103
Anti-human CD25 (clone 2A3) (149 Sm)	Standard BioTools Inc	Cat# 3149010B; RRID: AB_2756416
Anti-human IL-22 (clone 22URTI) (150 Nd)	Standard BioTools Inc	Cat# 3150007B; RRID: AB_2810972
Anti-human CD27 (clone LG.3A10) (150 Nd)	Standard BioTools Inc	Cat# 3150017B; RRID: N/A
Anti-human CD103 (clone Ber-ACT8) (151 Eu)	Standard BioTools Inc	Cat# 3151011B; RRID: AB_2756418
Anti-human CD38 (clone HIT2) (purified)	Biolegend	Cat# 303502; RRID: AB_314354
Anti-human TCRgd (clone 11F2) (152 Sm)	Standard BioTools Inc	Cat# 3152008B; RRID: AB_2687643
Anti-human CD25 (clone M-A251) (purified)	Biolegend	Cat# 356101; RRID: AB_2561751
Anti-human CD45RA (clone HI100) (153 Eu)	Standard BioTools Inc	Cat# 3153001B; RRID: AB_2802108
Anti-human IL-6 (clone MQ2-13A5) (purified)	Biolegend	Cat# 501101; RRID: AB_315149
Anti-human CD3 (clone UCHT1) (154 Sm)	Standard BioTools Inc	Cat# 3154003B; RRID: AB_2687853
Anti-human IL-9 (clone MH9A4) (purified)	Biolegend	Cat# 507602; RRID: AB_315484
Anti-human CD268 (clone 11C1) (155 Gd)	Standard BioTools Inc	Cat# 3155005B; RRID: N/A
Anti-human IL-13 (clone JES10-5A2) (purified)	Biolegend	Cat# 501901; RRID: AB_315196
Anti-human CXCR3 (clone G025H7) (156 Gd)	Standard BioTools Inc	Cat# 3156004B; RRID: AB_2687646
Anti-human CCR4 (clone 205410) (158 Gd)	Standard BioTools Inc	Cat# 3158006A; RRID: AB_2687647
Anti-human GM-CSF (clone BVD2-21C11) (159 Tb)	Standard BioTools Inc	Cat# 3159008B; RRID: AB_2864732
Anti-human CD116 (clone 4H1) (purified)	Biolegend	Cat# 305902; RRID: AB_314568
Anti-human CD69 (clone FN50) (purified)	Biolegend	Cat# 310902; RRID: AB_314837
Anti-human CD20 (clone 2H7) (purified)	Biolegend	Cat# 302301; RRID: AB_314249
Anti-human CD27 (clone O323) (purified)	Biolegend	Cat# 302802; RRID: AB_314294
Anti-human FOXP3 (clone PCH101) (162 Dy)	Standard BioTools Inc	Cat# 3162011A; RRID: AB_2687650
Anti-human CD7 (clone CD7-6B7) (purified)	Biolegend	Cat# 343102; RRID: AB_1659214
Anti-human CD45R0 (clone UCHL1) (164 Dy)	Standard BioTools Inc	Cat# 3164007B; RRID: AB_2811092
Anti-human IFNg (clone B27) (165 Ho)	Standard BioTools Inc	Cat# 3165002B; RRID: N/A
Anti-human CD127 (clone A019D5) (165 Ho)	Standard BioTools Inc	Cat# 3165008B; RRID: AB_2868401
Anti-human IL-10 (clone JES3-9D7) (166 Er)	Standard BioTools Inc	Cat# 3166008B; RRID: N/A
Anti-human CD86 (clone IT2.2) (purified)	Biolegend	Cat# 305401; RRID: AB_314521
Anti-human CCR7 (clone G043H7) (167 Er)	Standard BioTools Inc	Cat# 3167009A; RRID: AB_2858236
Anti-human TNF (clone MAb11) (purified)	Biolegend	Cat# 502901; RRID: AB_315253
Anti-human Ki67 (clone B56) (168 Er)	Standard BioTools Inc	Cat# 3168007B; RRID: AB_2800467

(Continued on next page)

Continued

REAGENT or RESOURCE	SOURCE	IDENTIFIER
Anti-human CD45RA (clone HI100) (169 Tm)	Standard BioTools Inc	Cat# 3169008B; RRID: N/A
Anti-human CD33 (clone WM53) (169 Tm)	Standard BioTools Inc	Cat# 3169010B; RRID: AB_2802111
Anti-human CD3 (clone UCHT-1) (170 Er)	Standard BioTools Inc	Cat# 3170001B; RRID: AB_2661807
Anti-human IgD (clone IA6-2) (purified)	Biolegend	Cat# 348202; RRID: AB_10550095
Anti-human CXCR5 (clone 51505) (171 Yb)	Standard BioTools Inc	Cat# 3171006B; RRID: AB_2938866
Anti-human CD22 (clone HIB22) (purified)	Biolegend	Cat# 302502; RRID: AB_314264
Anti-human IL-21 (clone 3A3-N2) (172 Yb)	Standard BioTools Inc	Cat# 3172011B; RRID: AB_2810975
Anti-human IgM (clone MHM-88) (172 Yb)	Standard BioTools Inc	Cat# 3172004B; RRID: AB_2810858
Anti-human CXCR4 (clone 12G5) (173 Yb)	Standard BioTools Inc	Cat# 3173001B; RRID: N/A
Anti-human CD56 (clone NCAM16.2) (purified)	BD Biosciences	Cat# 559043; RRID: AB_397180
Anti-human HLADR (clone L243) (174 Yb)	Standard BioTools Inc	Cat# 3174001B; RRID: AB_2665397
Anti-human CD28 (clone CD28.2) (purified)	Biolegend	Cat# 302902; RRID: AB_314304
Anti-human CD14 (clone M5E2) (175 Lu)	Standard BioTools Inc	Cat# 3175015B; RRID: AB_2811083
Anti-human CD56 (clone NCAM16.2) (176Yb)	Standard BioTools Inc	Cat# 3176008B; RRID: AB_2661813
Anti-human CD5 (clone UCHT2) (purified)	Biolegend	Cat# 300602; RRID: AB_314088
Anti-human CD16 (clone 3G8) (209 Bi)	Standard BioTools Inc	Cat# 3209002B; RRID: AB_2756431
Anti-human CD11b (clone ICRF44) (209 Bi)	Standard BioTools Inc	Cat# 3209003B; RRID: AB_2687654
Rabbit anti-CD27 (clone EPR8569)	Abcam	Cat# ab131254; RRID: AB_11155136
Mouse anti-CD3 (clone LN10)	Leica Microsystems	Cat# CD3-565-L-CE; RRID: AB_563541
Rabbit anti-CD70 (clone ERP26536-122)	Abcam	Cat# ab300083; RRID: AB_2924231
Rabbit anti-CD4 (clone SP35)	Ventana Medical Systems - Roche	Cat# 790–4423; RRID: AB_2335982
Goat anti-CD4 (polyclonal)	R&D	Cat# AF-379-SP; RRID: AB_354469
Mouse anti-CD20 (clone LN26)	Leica Microsystems	Cat# M0755; RRID: AB_2282030
mouse anti-CD20 (clone L26)	Ventana Medical Systems - Roche	Cat# 760–2531; RRID: AB_2335956
Donkey anti-mouse Alexa Fluor 488	Thermo Fisher Scientific	Cat# A21202; RRID: AB_141607
Donkey anti-goat Alexa Fluor 555	Thermo Fisher Scientific	Cat# A31572; RRID: AB_162543
Donkey anti-rabbit Alexa Fluor 647	Thermo Fisher Scientific	Cat# A21447; RRID: AB_2535864
Biological samples		
Cryopreserved PBMC samples	University Hospital Basel	
Cryopreserved PBMC samples	Karolinska University Hospital	
Brain tissue samples from relapsing MS with tumefactive brain lesions	University Hospital Zurich	
Chemicals, peptides, and recombinant proteins		
Phorbol 12-myristate 13-acetate	Sigma-Aldrich	Cat# P1585; RRID: N/A
Ionomycin	Sigma-Aldrich	Cat# I0634; RRID: N/A
Brefeldin A	BD Biosciences	Cat# 555029; RRID: N/A
Monensin	BD Biosciences	Cat# 554724; RRID: N/A
RPMI-1640	Biochrom	Cat# M 3413; RRID: N/A
L-glutamine	Thermo Fisher Scientific	Cat# 25030024; RRID: N/A
Penicillin–streptomycin	Thermo Fisher Scientific	Cat# 15140122; RRID: N/A
Cisplatin	Standard BioTools Inc	Cat# 201064; RRID: N/A
FOXP3 fixation/permeabilization buffer	Thermo Fisher Scientific	Cat# 00-5521-00; RRID: N/A
Saponin	Sigma-Aldrich	Cat# S7900; RRID: N/A
BSA	Sigma-Aldrich	Cat# B2064; RRID: N/A
FBS	Thermo Fisher	Cat# A3840002; RRID: N/A
Sodium azide	Sigma-Aldrich	Cat# 71290; RRID: N/A
PFA	Electron Microscopy Sciences	Cat# 15710; RRID: N/A
Iridium intercalator solution	Standard BioTools Inc	Cat# #201192B; RRID: N/A

(Continued on next page)

Continued

REAGENT or RESOURCE	SOURCE	IDENTIFIER
MaxPar water	Standard BioTools Inc	Cat# 201069; RRID: N/A
four-element beads	Standard BioTools Inc	Cat# 201078; RRID: N/A
DAKO Target Retrieval solution	Agilent	Cat# S2367; RRID: N/A
Blocking buffer (5% normal donkey serum/PBS + 0.1% Triton)	Southern Biotech	Cat# 0030-01; RRID: N/A
SlowFade Gold antifade reagent with DAPI	Thermo Fisher Scientific	Cat# S36938; RRID: N/A
Cell Conditioning Solution, Ultra CC1	Ventana Medical Systems - Roche	Cat# 950-224; RRID: N/A
Critical commercial assays		
OptiView DAB IHC Detection Kit	Ventana Medical Systems - Roche	Cat# 760-700; RRID: N/A
MaxPar X8 chelating polymer kit	Standard BioTools Inc	Cat# 201300; RRID: N/A
Deposited data		
Mass cytometry datasets	This paper	Ulutekin, Can (2023), "B cell depletion attenuates CD27 signaling of T helper cells in multiple sclerosis", Mendeley Data, V2, https://doi.org/10.17632/6hykgjvmn5.2
Github Repository	This paper	https://github.com/canulutekin/BCDT_MS
Zenodo DOI	This paper	https://zenodo.org/doi/10.5281/zenodo.10095377
Public single-cell RNA sequencing data	Schafflick et al.[32]	https://figshare.com/articles/dataset/MS_CSF_h5ad/14356661
Software and algorithms		
FlowJo V10.6.1.1	Tree Star	https://www.flowjo.com/
R version 4.2.2	R Development Core Team	https://www.r-project.org/
R Studio	RStudio Team	https://posit.co/products/open-source/rstudio/
CytoNorm	Van Gassen et al.[81]	https://github.com/saeyslab/CytoNorm
FlowSOM	Van Gassen et al.[82]	https://bioconductor.org/packages/release/bioc/html/FlowSOM.html
ConsensusClusterPlus	Wilkerson et al.[83]	https://bioconductor.org/packages/release/bioc/html/ConsensusClusterPlus.html
umap	McInnes et al.[84]	https://cran.r-project.org/web/packages/umap/index.html
Imaris imaging software v9.9	Oxford Instruments	https://imaris.oxinst.com/
Other		
CyTOF 2.1 Instrument	Standard BioTools Inc	
Ventana Benchmark Ultra autostainer	Ventana Medical Systems - Roche	
Microwave histoprocessor	HistosPro	
STELLARIS 5 microscope	Leica Microsystems	

RESOURCE AVAILABILITY

Lead contact
Further information and requests for resources and reagents should be directed to and will be fulfilled by the lead contact, Burkhard Becher (becher.immunology@uzh.ch).

Materials availability
This study did not generate new unique reagents.

Data and code availability
- Mass cytometry data generated during this study has been deposited at Mendeley Data and is publicly available. (Ulutekin, Can (2023), "B cell depletion attenuates CD27 signaling of T helper cells in multiple sclerosis", Mendeley Data, V2, https://doi.org/10.17632/6hykgjvmn5.2).

- All original code to replicate the analysis has been deposited at a public GitHub repository and is publicly available as of the date of publication. The repository is versioned and can be cited using Zenodo. Refer to the key resources table for further information.
- Any additional information required to reanalyze the data reported in this work paper is available from the lead contact upon request.

EXPERIMENTAL MODEL AND STUDY PARTICIPANT DETAILS

Longitudinal PBMC samples of MS patients during BCDT in the discovery cohort

For the initial discovery cohort longitudinal PBMC samples of MS patients before and after BCDT were collected at the MS center of the University Hospital Basel (Table S1). MS diagnosis was based on the revised McDonald criteria.[85] All patients gave written informed consent, with ethical oversight by the Ethikkommission beider Basel (Ref.Nr. EK: 49/06).

In the discovery cohort samples from multiple timepoints were available. Inclusion criteria for the discovery cohort included longitudinal patient samples, appropriate B cell depletion after BCDTs as well as no previous disruptive treatments.

In the analysis of non-B cells, we prioritized timepoints that met the inclusion criteria and were closest to the initial treatment cycle when selecting from the available post-treatment timepoints for each patient. We chose the first available timepoint after treatment for each patient, except in the case of patient 2. For this patient, the first available timepoint was only 14 days after their initial treatment, so the second timepoint was selected. For the analysis of the B cell compartment, we selected the post-treatment timepoint based on the highest B cell frequency, applying a 100-cell cut-off. Consequently, 8 out of 12 patients met the criteria for inclusion in the analysis.

All patients exhibited favorable outcomes with no clinical relapses or the observation of T2-lesions in MRI scans during the observation period after 6-month-rebaseline under BCDT, confirming a homogeneous clinical and radiological response among patients.

Longitudinal PBMC samples of MS and MG patients during BCDT in the validation cohort

Cryopreserved longitudinal PBMC samples of MS and MG patients before and after BCDT in the validation cohort were collected at the Department of Neurology at Karolinska University Hospital (Tables S2 and S3). MS patients were diagnosed according to the revised McDonald criteria.[85] The MG diagnosis was confirmed by at least 2 of the following: a positive AChR antibody test result, an abnormal electrophysiological test result (repetitive nerve stimulation and/or single fiber electromyography) consistent with MG, and/or a clinically significant response to an oral or intravenous AChEI test (per treating physician's opinion). All patients had given written informed consent, and the study has been approved by the regional ethical review board of Stockholm (MS dnr. 2009/2107-21/2, last amendment dnr. 2022-03650-02; MG 2016-827-31).

In the validation cohort each patient had one timepoint before treatment and one timepoint after treatment. Inclusion criteria for the validation cohort included appropriate B cell depletion after BCDTs. All patients exhibited favorable outcomes with no clinical relapses or the observation of T2-lesions in MRI scans during the observation period after 6-month-rebaseline under BCDT, confirming a homogeneous clinical and radiological response among patients.

Histology samples

Brain tissue from three individuals with MS was obtained from the archives of the Institute of Neuropathology at the University Hospital Zurich, Switzerland. All patients were diagnosed with relapsing MS with tumefactive brain lesions which were the reason for a diagnostic biopsy early during their disease. Case series do not need institutional review board approval according to Swiss legislation, however written informed consent for the publication of histological images was obtained from all three individuals.

METHOD DETAILS

Ex vivo activation of PBMCs from MS patients

For intracellular cytokine detection, PBMCs were activated as described previously.[86] In brief, PBMCs were stimulated with 50 ng/mL phorbol 12-myristate 13-acetate (Sigma-Aldrich), 500 ng/mL ionomycin (Sigma-Aldrich), 1× brefeldin A (BD Biosciences) and 1× monensin (BD Biosciences) in cell culture medium (RPMI-1640, 10% FBS (Biochrom), 1× L-glutamine (Thermo Fisher Scientific) and 1× penicillin–streptomycin (Thermo Fisher Scientific)) at 37°C for 4h. PBMCs were washed once in cell culture medium and barcoded subsequently.

Live cell barcoding for mass cytometry

PBMCs of both, the discovery, and the validation cohort, were processed and acquired in two independent batches each. Each batch contained PBMCs of a healthy donor that was used as normalization control to quantify batch effects between individual experiments. Longitudinal samples of the same patient were acquired in the same batch. Two panels were used to acquire the samples from the discovery cohort, one panel directed against surface epitopes of unmanipulated PBMCs and one panel to detect intracellular cytokines after *ex vivo* activation. The intracellular cytokine panel after *ex vivo* activation was used to acquire the samples from the validation cohort. Antibodies for metal isotopes were purchased from Standard Biotools Inc, Biolegend and BD Biosciences with

some being preconjugated and others in-house conjugated using the MaxPar X8 chelating polymer kit (Standard Biotools Inc). The full list of antigens per panel, clones of antibodies utilized, and heavy metal tags are listed in Tables S4–S6.

PBMCs of each individual batch were barcoded using a restricted live cell barcoding strategy as described before.[60] In short, anti-CD45 monoclonal antibodies were tagged with ^{89}Y, ^{104}Pd, ^{105}Pd, ^{106}Pd, ^{108}Pd, ^{110}Pd, ^{115}In and ^{181}Ta isotopes and a restricted 8-choose-3 barcoding scheme was applied (Tables S4–S6). PBMCs of each sample were labeled with a unique barcode consisting of three different heavy metal-tagged anti-CD45 antibodies in RPMI-1640 and 4% FBS for 25 min. Barcoded cells were washed twice with RPMI-1640 and 4% FBS and pooled into one single reaction vessel.

Surface and intracellular cytokine staining for mass cytometry
The barcoded sample convolute was labeled with a mix of antibodies directed against surface epitopes in RPMI-1640 and 4% FBS for 40 min at 37°C. Live/dead discrimination was achieved by incubating the sample convolute in 2.5 μM cisplatin (Standard BioTools Inc.) in PBS for 2 min on ice followed by the addition of 2% FBS in PBS for two more minutes.

For the antibody panel directed against surface epitopes of unmanipulated PBMCs, cells were fixed in 1X FOXP3 fixation/permeabilization buffer (Thermo Fisher Scientific) for 40 min at 4°C to facilitate transcription factor labeling. Cells were washed twice in with permeabilization buffer (0.5% saponin (Sigma-Aldrich), 2% BSA (Sigma-Aldrich), 0.01% sodium azide (Sigma-Aldrich) in PBS) and labeled with antibody mix in permeabilization buffer for 1 h at 4°C.

For the antibody panel directed against intracellular cytokines, cells were fixed in 1.6% PFA (Electron Microscopy Sciences) for 1h at 4°C washed with permeabilization buffer. Cells were incubated with the antibody mix directed against cytokines in permeabilization buffer for 1 h at 4°C.

For both panels, PBMCs were washed in PBS and incubated in 1X iridium intercalator solution (Standard BioTools Inc.) at 4°C overnight. Cells were washed twice with PBS and twice with MaxPar water (Standard BioTools Inc.).

Mass cytometry data acquisition and preprocessing
The barcoded sample convoluted for each panel and cohort was acquired in two independent batches. Each batch was acquired on a CyTOF 2.1 (Standard BioTools Inc.) and instrument performance and tuning were checked on a daily basis. Data were normalized using four-element beads (Standard BioTools Inc.).[87] Live singlets were identified by manual gating based on the parameters event length, center, width, DNA content ($^{191/193}$Ir) and live/dead staining (^{195}Pt) in FlowJo (BD Biosciences). Living cells in the sample convolute were debarcoded by applying manual Boolean gates in FlowJo (BD Biosciences). Only cells bearing exactly three distinct metal barcodes were extracted to exclude doublets and prevent misidentification of barcodes. To address the relative intensities in our debarcoded mass cytometry data, we performed data transformation in R using a hyperbolic arcsin function and derived cofactors for each marker following established methodologies.[88] The data was normalized between 0 and 1 using the 99.95th percentile.

Batch normalization
A batch effect was observed in the data obtained using the cytokine panel across two independent acquisitions. Longitudinal samples of patients were present within the same batch, as such, this batch effect was most impactful during clustering, generating batch specific clusters. To minimize the effect, batch normalization was done using the R package "CytoNorm".[81] The training and application of the algorithm was done just after the transformation of the data. Healthy donor samples present in both batches were used to train the algorithm, and no marker was excluded from normalization. The normalization was quality tested using biaxial plots sequentially checking for all clusters, to ensure there was no splitting or merging of valid populations.

High-dimensional analysis
The data was initially clustered using the R package "FlowSOM"[82] and generated 100 clusters based on the expression of all available markers except for cytokines. The "ConsensusClusterPlus"[83] package was used subsequently to sequentially merge the clusters until 30 clusters were achieved. To identify biologically meaningful cell types, the final clusters were merged manually and annotated based on marker expression characteristics. Common lineage markers were used for the merging and annotation of subsets (Figure S3). In the analysis of CSF data from Schafflick et al.,[32] we employed cluster annotations as defined in the original study.

Immunostaining of human brain tissue
For IHC examination, 2-3 μm-thick sections were tested using Ventana Benchmark Ultra autostainer (Ventana Medical Systems - Roche). After dewax and pretreatment (antigen retrievals with Cell Conditioning Solution, Ultra CC1, Ventana Medical Systems - Roche), samples were incubated with mouse anti-CD3 (clone LN10, Leica Microsystems), rabbit anti-CD4 (clone SP35, Ventana Medical Systems - Roche), and mouse anti-CD20 (clone L26, Ventana Medical Systems - Roche) antibodies. Primary antibodies were visualized using the OptiView DAB IHC Detection Kit (Roche).

Immunofluorescence stainings: For epitope demasking, deparaffinized sections were heated in a microwave histoprocessor (HistosPro) with DAKO Target Retrieval solution pH 9.0 (S2367, Agilent), washed and subsequently incubated with blocking buffer (5% normal donkey serum/PBS + 0.1% Triton) for 30–60 min. The following primary antibodies were used: Rabbit anti-CD27 (abcam, clone EPR8569, dilution 1:500) was combined with mouse anti-CD3 (Leica Microsystems Ltd, clone LN10, dilution 1:500) and goat anti-CD4 (R&D, polyclonal, dilution 1:50) to co-label CD4$^+$ T cells. In addition, rabbit anti-CD70 (abcam, clone ERP26536-122, dilution

1:100) was combined with mouse anti-CD20 (Leica Microsystems Ltd, clone LN26, dilution 1:100) and goat anti-CD4. The secondary antibody mixture contained donkey anti-mouse Alexa Fluor 488, anti-goat Alexa Fluor 555 and anti-rabbit Alexa Fluor 647 (all purchased from Thermo Fisher Scientific; dilution 1:250). Nuclear counterstaining was performed using SlowFade Gold antifade reagent with DAPI (Thermo Fisher Scientific). Imaging was performed on an STELLARIS 5 (Leica Microsystems Ltd) microscope with a ×20 or ×40 multi-immersion objective. Imaris imaging software v9.9 (Oxford Instruments) was used for image processing. Imaging was performed with equipment maintained by the Center for Microscopy and Image Analysis, University of Zurich.

QUANTIFICATION AND STATISTICAL ANALYSIS

All statistical analyses were done in R. Comparisons between groups were done using the non-parametric paired Wilcoxon rank-sum test. Corrections for multiple hypothesis testing were done using the Benjamini-Hochberg method. Statistical methods are indicated in the figure legends. The R package "umap"[84] was used to generate the UMAP coordinates. The R packages "ComplexHeatmap" and "ggplot2" were used for the visualizations of the data in various plots. The R packages "flowCore", "dplyr", "tidyr" and "tibble" were used for loading and reformatting the data. The R package "Seurat" was used in the analysis of publicly available single-cell RNA sequencing data.